文章编号:1000-8055(2021)01-0119-11 doi:10.13224/j.cnki.jasp.2021.01.014

Hover performance of helicopter main and tail rotors with swirl velocities

YANG Kelong, HAN Dong

(National Key Laboratory of Science and Technology on Rotorcraft Aeromechanics, College of Aerospace Engineering, Nanjing University of Aeronautics and Astronautics, Nanjing 210016, China)

Abstract: It is important to quickly predict the hover performance of main and tail rotors with sufficient precision for helicopter design. To investigate the effects of swirl velocities on the hover performance of main and tail rotors, and give a better prediction for the hover performance, a flight performance model was derived and a swirl velocity model was coupled into it. The test data of the UH-60A helicopter were used for validation. When the blade loading coefficient of the main rotor was higher than 0.05, the effects of the swirl velocities on the main rotor power became significant. The swirl velocities increased the profile torque of the main rotor. The increased torque required the tail rotor to produce more thrust with more power consumption. At a higher blade loading coefficient of the main rotor of 0.12, the swirl velocities increased the main rotor power, tail rotor power and total power by 3.80%, 5.24% and 5.08%, respectively. The profile power increase of the main rotor caused by the profile swirl velocity was less than that of the induced swirl velocity, but the power increase was higher at high rotor blade loadings. Considering the swirl velocities in the main rotor can improve the prediction precision of the hover performance, especially at high blade loadings.

Key words: swirl velocities; hover performance; main and tail rotors; blade loading; rotor power

CLC number: V211.52 **Document code**: A

Fast predict the hover performance of main and tail rotors with sufficient precision is important for helicopter design. Many methods have been used to predict the hover performance, such as momentum theory (MT), computational fluid dynamics (CFD) and blade element theory (BET). The MT provides a preliminary evaluation of hover performance. The CFD can better predict the rotor performance with a high number of computing resources. The BET is a practical approach for the rotor design and performance prediction, which can balance the prediction precision and computing time. However, the performance prediction method based on the BET is usually simplified, which results in a higher difference between the prediction and the flight test data[1-3]. For example, the BET usually considers the axial induced inflow while omits the swirl velocities over the rotor disk. The swirl velocities are usually considered in performance prediction of propellers and proprotors, which usually operates at high blade loading state[4-5]. To better predict the hover performance by the BET, it is necessary to explore the effect of the swirl velocities on the performance of the main and tail rotors, especially at high blade loadings.

Johnson[6] derived an approximate relation between the swirl velocities and the main rotor power at low thrust. The derivation was based

Received: 2020-06-14

Foundation items: National Natural Science Foundation of China (11972181); the Six Talent Peaks Project in Jiangsu Province (GDZB-013); the Open Research Foundation of the Key Rotor Aerodynamics Laboratory (2005RAL20200104)

Citation: YANG Kelong, HAN Dong. Hover performance of helicopter main and tail rotors with swirl velocities[J]. Journal of Aerospace Power, 2021, 36(1): 119-129.

on the conservation of energy and angular momentum. The analysis indicated that the rotor induced torque and profile torque could induce an induced swirl velocity and a profile swirl velocity. The induced swirl velocity and profile swirl velocity constituted the swirl velocities. The power increase of the main rotor was less than 1.0% at low thrust caused by the swirl velocities. Lucas[7] considered the induced swirl velocity in a coaxial rotor model based on the BET. The swirl velocity contributed to a 2.1% increase of the total power at a low take-off weight of 7 942.5 kg. Stahlhut and Leishman[8] considered the induced swirl velocity in a proprotor athigh-speed flight. The operation state of the proprotor was similar to a propeller (i. e. the proprotor operated in an axial inflow state). At high advance ratios, the induced swirl velocity was critical to better predict performance. Modarres and Peters[9] analyzed the rotor performance in hover and axial flight by a compact MT with induced swirl velocity. The analysis was based on an actuator-disk model. The figure of merit (η) reduction caused by the induced swirl velocity was less than 0.6% when the thrust coefficient was lower than 0.05. In reviewing the literatures, most studies mainly investigate the effects of the induced swirl velocity on the main rotor performance at low thrust.

In this work, a prediction model of the flight performance for a helicopter is derived. The prediction model is validated by the flight test data of a UH-60A helicopter. A swirl velocities model is also derived and coupled into the prediction model of the flight performance, which considers the profile swirl velocity on the hover. The effects of the swirl velocities on the hover performance of the main and tail rotors are investigated, especially at high blade loadings. The potential of considering the swirl velocities for improving prediction precision of the rotor performance by the BET is also investigated.

1 Flight performance modeling

In this section, a flight performance model for hover and forward is derived. And a swirl velocity model (derived in section 3) will be coupled into the flight performance model.

The flight performance model includes a main rotor model, a tail rotor model and a fuselage model. To reduce the effect of elastic deformation of main rotor blade on the induced velocities, the blade is modeled as a rigid beam with a hinge offset and a hinge spring. Peters, et al.[10] dynamic inflow model is utilized to predict the induced velocity over the main rotor disk. The lift coefficient C_l and drag coefficient C_d of blade airfoil segments are interpolated from nonlinear lookup tables, which can consider the compressibility effects of the blade airfoil segments. As shown in Fig. 1, the lift L and drag D on an airfoil segment are

$$\begin{cases} \mathrm{d}L = \dfrac{1}{2}\rho U^2 c C_l \mathrm{d}r \\ \mathrm{d}D = \dfrac{1}{2}\rho U^2 c C_d \mathrm{d}r \end{cases} \tag{1}$$

Where, ρ is the air density, c is the chord length of the airfoil segment, r is the radial location of the airfoil segment of the main rotor blade, and U is the resultant velocity given by

$$U = \sqrt{U_p^2 + U_t^2} \tag{2}$$

Where, U_p is the out-of-plane velocity normal to the main rotor disk, and U_t is the in-plane velocity parallel to the main rotor disk.

Resolving the lift and drag perpendicular and parallel to the main rotor disk plane gives:

$$\begin{cases} \mathrm{d}F_x = -(\mathrm{d}L\sin\phi + \mathrm{d}D\cos\phi) \\ \mathrm{d}F_y = 0 \\ \mathrm{d}F_z = \mathrm{d}L\cos\phi - \mathrm{d}D\sin\phi \end{cases} \tag{3}$$

Where, ϕ is the inflow angle which is the difference between the pitch angle θ and angle of attack (AoA) α.

Transforming the $\mathrm{d}F_x$, $\mathrm{d}F_y$ and $\mathrm{d}F_z$ to the main rotor shaft coordinate frame (denoted by a superscript "s"), the components of the aerodynamic forces are

$$\begin{cases} \mathrm{d}F_x^s = \mathrm{d}F_z\sin\beta\cos\psi - \mathrm{d}F_x\sin\psi \\ \mathrm{d}F_y^s = -\mathrm{d}F_z\sin\beta\sin\psi - \mathrm{d}F_x\cos\psi \\ \mathrm{d}F_z^s = \mathrm{d}F_z\cos\beta \end{cases} \tag{4}$$

Where, β is the flapping angle of the blade, and ψ is the azimuth angle of blade.

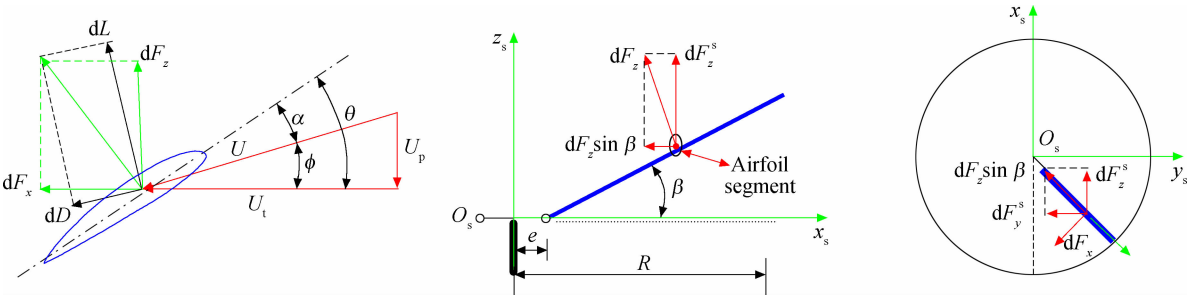

Fig. 1　Forces on airfoil segment of blade in coordinate frame of main rotor

By integrating these forces along the radial direction of the blade first, and then the azimuth direction, the thrust T_{mr}, drag H_{mr} and side force Y_{mr} of the main rotor can be obtained by

$$\begin{cases} T_{mr} = \dfrac{N_b}{2\pi}\displaystyle\int_0^{2\pi}\int_e^R \mathrm{d}F_z \mathrm{d}\psi \\ H_{mr} = \dfrac{N_b}{2\pi}\displaystyle\int_0^{2\pi}\int_e^R (\mathrm{d}F_x \sin\psi + \mathrm{d}F_y \cos\psi)\mathrm{d}\psi \\ Y_{mr} = \dfrac{N_b}{2\pi}\displaystyle\int_0^{2\pi}\int_e^R (-\mathrm{d}F_x \cos\psi + \mathrm{d}F_y \sin\psi)\mathrm{d}\psi \end{cases} \tag{5}$$

Where, N_b is the number of the main rotor blades, e is the flapping hinge offset, and R is the main rotor radius.

The torque Q_{mr}, roll moment $M_{x,mr}$, and pitch moment $M_{y,mr}$ of the main rotor are

$$\begin{cases} Q_{mr} = \dfrac{N_b}{2\pi}\displaystyle\int_0^{2\pi}\int_e^R r\mathrm{d}F_x \mathrm{d}\psi \\ M_{x,mr} = \dfrac{N_b}{2\pi}\displaystyle\int_0^{2\pi}\int_e^R r\mathrm{d}F_z \sin\psi \mathrm{d}\psi \\ M_{y,mr} = -\dfrac{N_b}{2\pi}\displaystyle\int_0^{2\pi}\int_e^R r\mathrm{d}F_z \cos\psi \mathrm{d}\psi \end{cases} \tag{6}$$

The tail rotor thrust is obtained by integrating the forces and of the airfoils along the radial direction of the blade first and then the azimuth direction. The fuselage is considered as a rigid body with aerodynamic forces and moments. These forces and moments acting on a helicopter are shown in Fig. 2 at a forward speed V, which constitutes the helicopter equilibrium equations[11]:

$$\begin{cases} \sum F_x = 0 \quad D_f + H_{mr} - T_{mr}\theta_f = 0 \\ \sum F_y = 0 \quad Y_{mr} + T_{tr} + T_{mr}\phi_f = 0 \\ \sum F_z = 0 \quad W - T_{mr} = 0 \\ \sum M_x = 0 \quad M_{x,mr} + M_{x_f} + W(h\phi_f - y_{cg}) + T_{tr}h_{tr} = 0 \\ \sum M_y = 0 \quad M_{y,mr} + M_{y_f} + W(h\theta_f - x_{cg}) - D_f h = 0 \\ \sum M_z = 0 \quad Q_{mr} - T_{tr}l_{tr} = 0 \end{cases} \tag{7}$$

Where, D_f is the fuselage drag. θ_f is the fuselage pitch angle. T_{tr} is the tail rotor thrust. ϕ_f is the fuselage roll angle. W is the take-off weight. h is the vertical distance from the gravity center of the helicopter to the main rotor hub, and h_{tr} is the vertical distance from the gravity center of the helicopter to the tail rotor hub. M_{x_f} and M_{y_f} are the roll and pitch moment of fuselage. $x\alpha_{cg}$

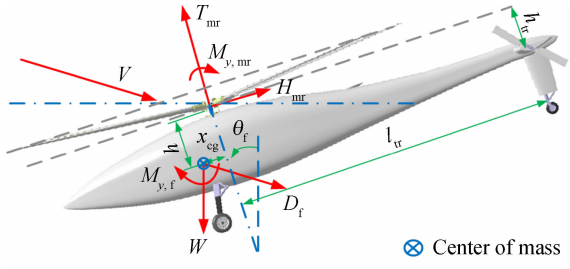

(a) Longitudinal forces and moments

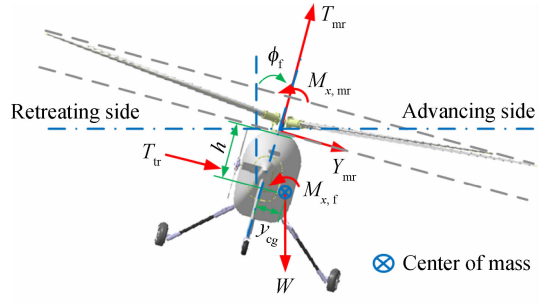

(b) Lateral forces and moments

Fig. 2　Forces and moments acting on a helicopter

and y_{cg} are the longitudinal and lateral distances from the gravity center of the helicopter to the main rotor hub. l_{tr} is the longitudinal distance from the tail rotor hub to the main rotor hub. More details of the flight performance modeling can refer to Refs. [12-14].

2 Validation

The flight data of a UH-60A helicopter[15-16] are utilized to validate the flight performance model. The parameters of the helicopter are given in Table 1 and Table 2[17-18]. The fuselage drag equation from Ref. [15] is utilized in this work:

$$\frac{D_f}{q} = 35.83 + 0.016 \times (1.66\theta_f^2) \tag{8}$$

Where, q is the dynamic pressure.

Fig. 3 shows the comparison of the main and tail rotors power between the predictions and the flight test data. The predictions by the present model are generally in good agreement with the flight test data at the take-off weight coefficients (C_w) of 0.0074 and 0.0083.

Table 1 Main rotor parameters

Parameter	Values and description
Main rotor radius/m	8.178
Root cutout/m	1.066
Flap hinge offset/m	0.3817
Number of blades	4
Main rotor speed/(rad/s)	27.0
Blade chord length/m	Nonlinear
Blade twist/(°)	Nonlinear
Airfoil	SC 1095/SC 1094 R8
Blade mass/(kg/m)	13.9

Table 2 Tail rotor parameters

Parameter	Values and description
Tail rotor radius/m	1.6764
Number of blades	4
Tail rotor speed/(rad/s)	124.62
Tail rotor blade chord/m	0.2469
Tail rotor blade twist/(°)	−18
Airfoil	SC 1095

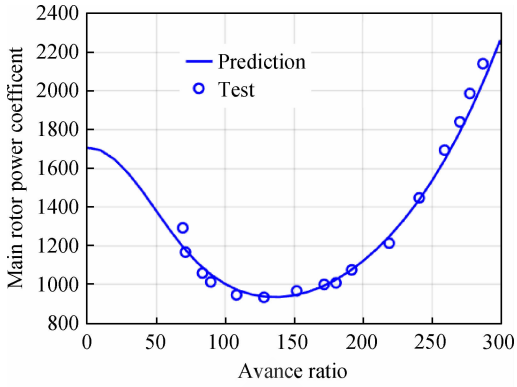

(a) Main rotor power coefficient, C_w=0.0074

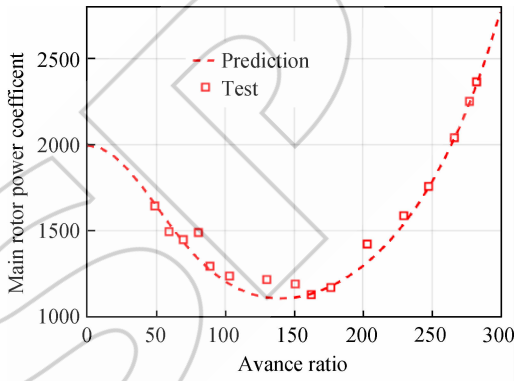

(b) Main rotor power coefficient, C_w=0.0083

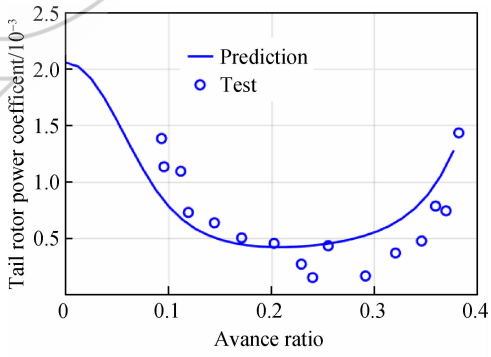

(c) Tail rotor power coefficient, C_w=0.0074

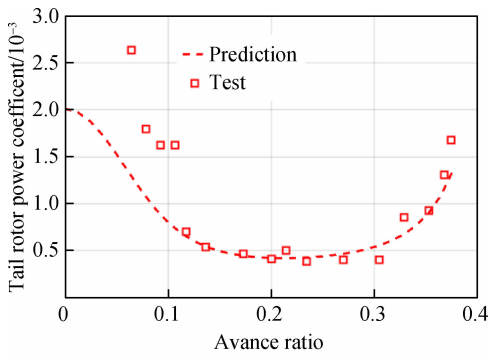

(d) Tail rotor power coefficient, C_w=0.0083

Fig. 3 Comparisons of the main and tail rotors power between the predictions and flight test data

3 Swirl velocities modeling in hover

The modeling of the swirl velocities can refer to Ref. [19]. The rotor torque Q consists of the induced component Q_i and the profile component Q_0. The conservation of the angular momentum gives the relation between the rotor torque and the swirl velocities u as

$$dQ = dQ_i + dQ_0 = \rho v_i u r dA \tag{9}$$

Where, v_i is the axial induced velocity, u is swirl velocity, and dA is the area of an annulus of the rotor disk.

The induced torque dQ_i can be expressed as

$$dQ_i = \frac{dP_i}{\Omega} \tag{10}$$

Where, Ω is rotor velocity. P_i is rotor induced power. The relation between P_i and the swirl velocity u is derived from the conservation of energy as

$$dP_i = \Delta p v_i dA + \frac{1}{2}\rho v_i u^2 dA \tag{11}$$

Where, Δp is a uniform pressure difference across the rotor disk. Δp equals the rotor disk loading

$$\Delta p = \frac{dT}{dA} = \frac{1}{2}\rho(2v_i)^2 \tag{12}$$

Where, dT is the thrust of an annulus of the rotor disk.

The BET gives the expression of the profile torque Q_0

$$dQ_0 = N_b r dD \cos\phi = N_b r \frac{C_d}{C_l} dL \cos\phi = r\frac{C_d}{C_l} dT \tag{13}$$

The $dP_i = \Omega dQ_i$ becomes

$$\Delta p v_i dA + \frac{1}{2}\rho v_i u^2 dA = \left(\rho v_i u r dA - r\frac{C_d}{C_l} dT\right) \tag{14}$$

Substituting Eq. (12) into Eq. (14), the above equation becomes

$$\left(\frac{1}{2}u - \Omega r\right)\frac{1}{2}u + v_i^2 + \frac{C_d}{C_l}\Omega r v_i = 0 \tag{15}$$

At any given radial location, the swirl velocities can be obtained by solving Eq. (15), which is added in the tangential velocity in the aerodynamics. The above velocities and forces of an airfoil segment on the annulus over rotor disk are shown in Fig. 4. The resultant velocity U is given by

$$U = \sqrt{U_p^2 + U_t^2} = (\Omega r - u)^2 + v_i^2 \tag{16}$$

Since the swirl velocity model is derived by the combined blade element momentum theory, the model is applicable to hover performance prediction.

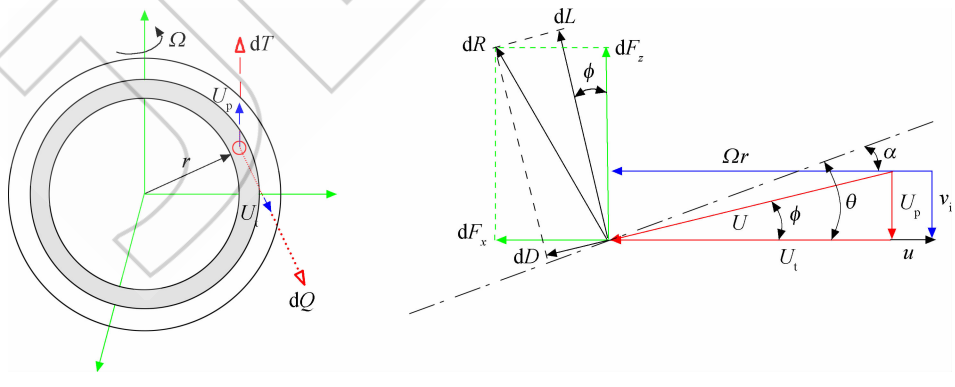

Fig. 4　Velocities and forces of an airfoil segment on the annulus over rotor disk

4 Prediction method

Fig. 5 shows the prediction flowchart of the hover performance with the swirl velocities. First, the flight altitude, take-off weight, initial values of fuselage attitude angles, pitch controls of the main and tail rotors, and the induced velocity model are given. The induced velocity model includes the swirl velocities model and axial induced model. Then the steady forces and moments of the fuselage, main and tail rotors can be obtained by the given initial values. Finally, the equilibrium equations can be solved, and the main and tail rotors power can also be derived.

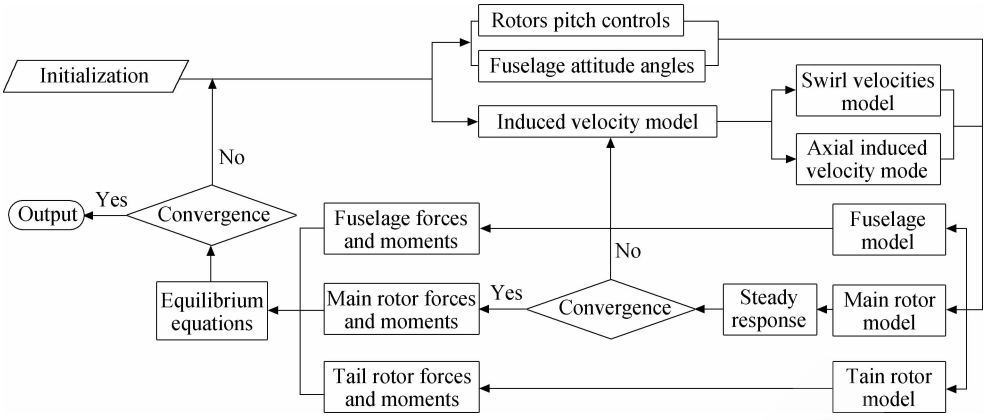

Fig. 5 Prediction flowchart of the hover performance with swirl velocities

5 Hover performance

The hover performance is evaluated by the η

$$\eta = \frac{C_t^{\frac{2}{3}}}{\sqrt{2}C_q} \tag{17}$$

Where, C_t and C_q are thrust and torque coefficients of the main rotor.

The power increase ratio caused by the swirl velocities is defined as

$$\gamma = \left(\frac{P}{P_b} - 1\right) \times 100\% \tag{18}$$

Where, P is the main rotor power, tail rotor power or total power considering the swirl velocities. P_b is the baseline main rotor power, tail rotor power or total power without considering the swirl velocities at sea level.

5.1 Main rotor

Fig. 6 shows the comparisons of the η between the predictions and the test data[20-21]. The 1st and 12th year data vary from each other by 0.02 to 0.04 in the η. The exact cause for these differences are discussed in Ref. [22]. When the blade loading coefficient of the main rotor C_t/σ (σ is rotor solidity) is lower than 0.005, the swirl velocities have little effect on the η. The predictions of the η with and without the swirl velocities show good agreement with the wind tunnel test data. When the C_t/σ is higher than 0.05, the effect of the swirl velocities on the η gradually becomes significant. When the C_t/σ is higher than 0.08, the baseline prediction gives a higher value than the test data. The prediction with swirl velocities lowers the baseline η. Considering the swirl velocities gives a more accurate prediction than the baseline, which shows better agreement with 1st year flight test data. When the $C_t/\sigma = 0.12$, the baseline η is 0.79, and η with swirl velocities is 0.76, a decrease of 3.80% caused by the swirl velocities. Considering the swirl velocities in the main rotor can improve the prediction precision, especially at high C_t/σ.

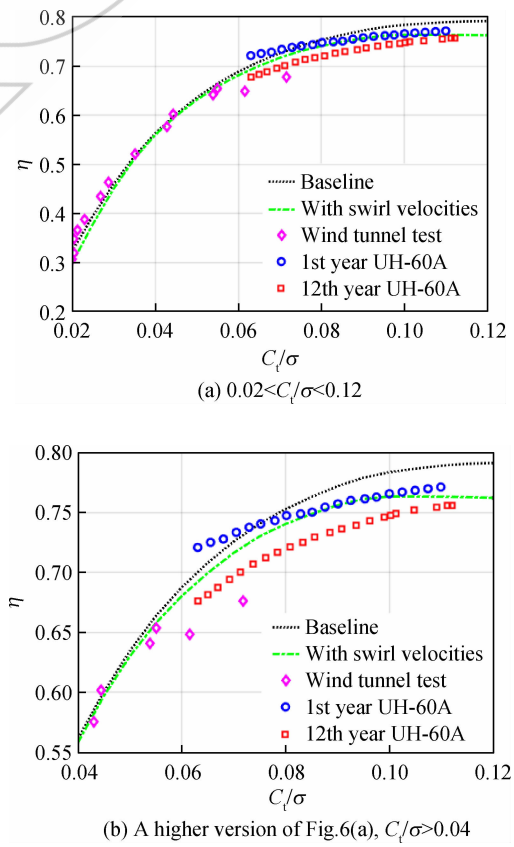

Fig. 6 Comparison of the η between the predictions and the test data

Fig. 7 shows the power increase of the main rotor caused by the swirl velocities. The power increases as increasing the C_t/σ. When the $C_t/\sigma = 0.06$, the swirl velocities only increase the main rotor power by 1.0%. The swirl velocities have little effect on the rotor power at low C_t/σ. When the $C_t/\sigma = 0.12$, the swirl velocities increase the rotor power by 3.80%. The induced swirl velocity contributes a 2.74% increase while the profile swirl velocity contributes a 1.13% increase of the main rotor power. Since the induced rotor torque is higher than the rotor profile torque, the induced swirl velocity contributes most of the rotor power increase.

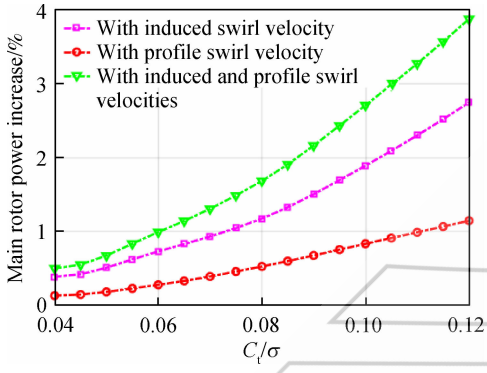

Fig. 7　Power increase of the main rotor caused by the swirl velocities

Fig. 8 shows the profile power increase of the main rotor caused by the swirl velocities. Since the induced power of the main rotor is determined by the C_t/σ. At the same C_t/σ, the swirl velocities little affect the induced power. The swirl velocities mainly increase the profile power. When the $C_t/\sigma = 0.12$, the swirl velocities increase the profile power of the main rotor by 10.32%. The induced swirl velocity contributes a 7.30% increase while the profile swirl velocity contributes a 3.02% increase of the main rotor power. Since the induced rotor torque is higher than the profile torque of the main rotor, the induced swirl velocity mainly contributes most of the rotor power increase. The power increase caused by the profile swirl velocity is smaller than that of the induced swirl velocity. The profile power increase caused by the profile swirl velocity is obvious when the C_t/σ is higher than 0.10. The swirl velocities significantly increase the profile power at high C_t/σ.

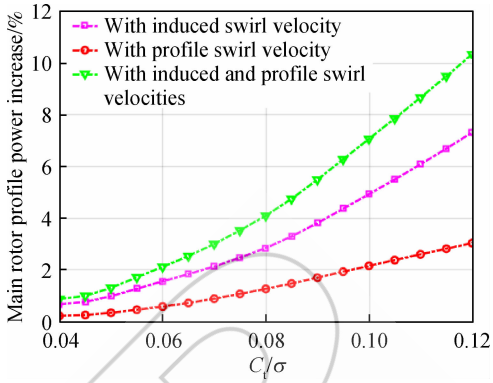

Fig. 8　Profile power increase of the main rotor caused by the swirl velocities

Fig. 9 showsthe distribution of the AoA and lift-to-drag ratio (L/D) of the blade airfoil segments over the main rotor disk with and without the swirl velocities. The swirl velocities increase the AoA and the stall region. For an airfoil segment, the swirl velocities decrease the tangential velocity U_t, which increases the inflow angle ϕ and decreases the AoA and C_t/σ. The main rotor collective pitch is increased to provide the same thrust to trim the helicopter, which leads to a higher AoA than the baseline, especially at high C_t/σ. The higher AoA increases the drag and lowers the L/D of the blade airfoil segments, which further increases the rotor profile torque. At a same thrust, the main rotor have to consumes more power to overcome these adverse effects due to the swirl velocities.

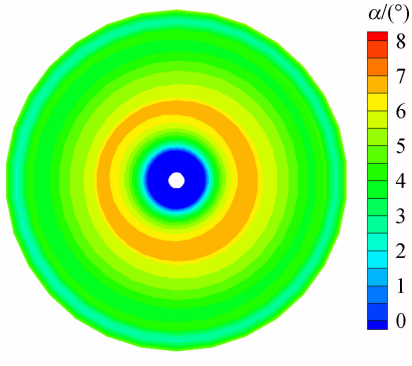

(a) AoA, baseline

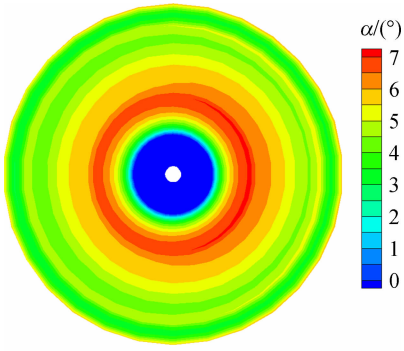

(b) AoA, with swirl velocities

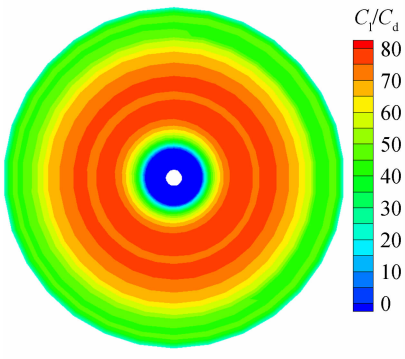

(c) L/D, baseline

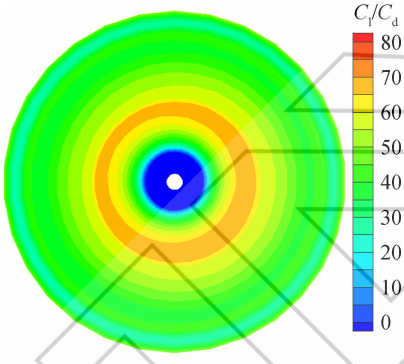

(d) L/D, with swirl velocities

Fig. 9 Distribution of the AoA and L/D of the blade airfoil segments over the main rotor disk ($C_t/\sigma=0.12$)

5.2 Tail rotor

Fig. 10 shows the relation of the blade loading coefficient between the main rotor and tail rotor for a trimmed helicopter (the swirl velocities are not considered). The blade loading coefficient of the tail rotor of $C_{t,tr}/\sigma_{tr}$ ($C_{t,tr}$ and σ_{tr} are the tail rotor thrust coefficient and solidity) increases as increasing the C_t/σ. The increased C_t/σ demands the tail rotor to provide larger thrust to overcome the main rotor torque. When $C_t/\sigma=0.12$, the $C_{t,tr}/\sigma_{tr}$ can reach 0.138. The above analysis in section 5.1 indicates that the swirl velocities have a significant effect on the main rotor performance at high C_t/σ. The tail rotor usually operates at a higher blade loading state with smaller rotor radius and higher rotor speed than the main rotor. The effects of the swirl velocities on the hover performance of the tail rotor may be more significant. The performance of the tail rotor dominants the efficiency of yaw control and balancing the main rotor torque. It is necessary to investigate the effects of the swirl velocities on the hover performance of the tail rotor.

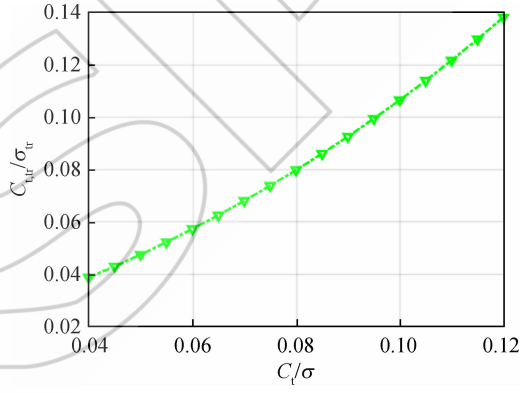

Fig. 10 Relation of the blade loading coefficient between the main rotor and tail rotor (without considering the swirl velocities)

Fig. 11 shows the power increase of the tail rotor caused by the swirl velocities. The power increases rapidly as increasing the $C_{t,tr}/\sigma_{tr}$. The swirl velocities little affect the rotor power at low $C_{t,tr}/\sigma_{tr}$. When the $C_{t,tr}/\sigma_{tr}=0.138$ (the corresponding C_t/σ is 0.012), the power increase

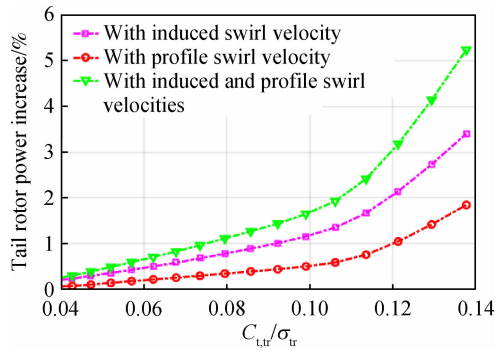

Fig. 11 Power increase of the tail rotor caused by the swirl velocities

can reach 5.24%. The induced swirl velocity contributes a 3.40% increase while the profile swirl velocity contributes a 1.84% increase of the tail rotor power. The swirl velocities have a more significant effect on the performance than that of the main rotor.

Fig. 12 shows the profile power increase of the tail rotor caused by the swirl velocities. At higher $C_{t,tr}/\sigma_{tr}$, the swirl velocities significantly increase the profile power. When the $C_{t,tr}/\sigma_{tr}=0.138$, the swirl velocities increase the tail rotor power by 12.84%. The induced swirl velocity contributes a 8.33% increase while the profile swirl velocity contributes a 4.51% increase of the tail rotor power. The profile power increase caused by the profile swirl velocity is obvious when the $C_{t,tr}/\sigma_{tr}$ is higher than 0.10. The higher tail rotor speed increases the tail rotor profile torque. The higher profile torque will induce a larger profile swirl velocity, which results in a larger increase of profile power at high $C_{t,tr}/\sigma_{tr}$.

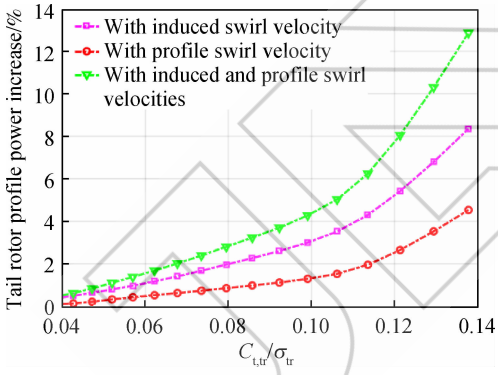

Fig. 12　Profile power increase of the tail rotor caused by the swirl velocities

5.3　Main and tail rotors

Fig. 13 shows the power increase of the tail rotor caused by the swirl velocities over the main rotor disk. The tail rotor power increases as increasing the C_t/σ. When the C_t/σ is lower than 0.08. The swirl velocities over the main rotor disk has little effect on the tail rotor power. At a higher C_t/σ of 0.12, the swirl velocities increase the tail rotor power by 5.74%. The swirl velocities over the main rotor disk increases the main rotor torque. The tail rotor will produce more thrust to balance the main rotor torque with more power consumption. At lower C_t/σ, the power increase of the tail rotor can be omitted, but the power increase is obvious at higher C_t/σ.

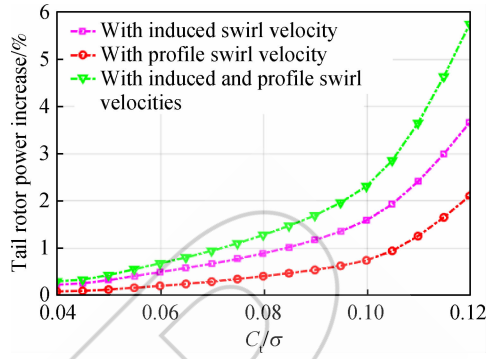

Fig. 13　Power increase of the tail rotor caused by the swirl velocities over the main rotor disk

Fig. 14 shows the total power increase of the main and tail rotors caused by the swirl velocities. The total power increases as increasing the C_t/σ. When the $C_t/\sigma=0.08$, the swirl velocities increase the total power by 1.72%. At a higher C_t/σ of 0.12, the swirl velocities increase the total power by 5.08%. The induced swirl velocity increases the total power by 3.45%. The profile swirl velocity increases the total power by 1.63%. The swirl velocities significantly increase the total power at high C_t/σ, especially the induced swirl velocity.

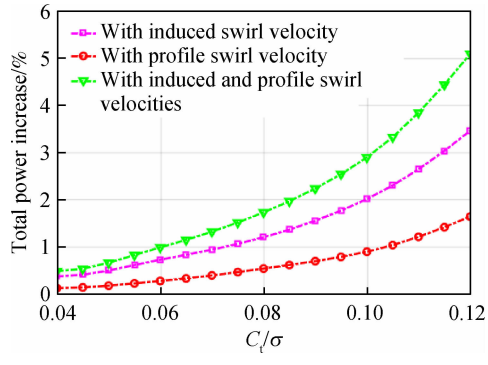

Fig. 14　Total power increase of the main and tail rotors caused by the swirl velocities

6　Conclusions

This work focuses on the effects of the swirl velocities on the hover performance of the main

and tail rotors. First, a prediction model of the flight performance for a helicopter is derived based on the blade element theory. The model consists of a main rotor model, a tail rotor model and a fuselage model. Next, prediction model the flight performance is validated by the flight test data of a UH-60A helicopter, which shows good agreement with the flight test data. Then, a swirl velocities model is derived and coupled into the prediction model of the flight performance. Finally, the effects of the swirl velocities on the hover performance of the main and tail rotors are investigated, especially at high blade loadings. The analysis yielded the following conclusions:

1) At low C_t/σ, the swirl velocities have little effect on the η. The predictions of the η with and without the swirl velocities show good agreement with the wind tunnel test data.

2) When the C_t/σ is higher than 0.05, The effect of the swirl velocities on the η gradually becomes significant. When the $C_t/\sigma=0.12$, the swirl velocities increase the main rotor power by 3.80%. Considering the swirl velocities in the main rotor can improve the prediction precision, especially at high blade loading.

3) When the $C_{t,tr}/\sigma_{tr}=0.138$, the swirl velocities increase the tail rotor power by 5.24%. The induced swirl velocity contributes a 3.40% increase while the profile swirl velocity contributes a 1.84% increase of the power. The profile power increase due to the profile swirl velocity is less than that of the induced swirl velocities, but the power increase is at high C_t/σ.

4) The swirl velocities over the main rotor disk increases the main rotor torque. The tail rotor will produce more thrust to balance the main rotor torque with more power consumption. At a higher C_t/σ of 0.12, the swirl velocities increase the tail rotor power by 5.74%.

5) The swirl velocities over the main and tail rotor disks have obvious effect on the total power. At a higher C_t/σ of 0.12, the swirl velocities increase the total power by 5.08%. The induced swirl velocity increases the total power by 3.45%. The profile swirl velocity increases the total power by 1.63%. The swirl velocities significantly increase the total power at high C_t/σ.

References:

[1] LIM J W, MCALISTER K W, JOHNSON W R. Hover performance correlation for full-scale and model-scale coaxial rotors[J]. Journal of the American Helicopter Society, 2009, 54(2): 1-14.

[2] JAIN R K, POTSDAM M A. Hover predictions on the Sikorsky S-76 rotor using helios[C]// 52nd Aerospace Sciences Meeting. Virginia Beach, US: AIAA, 2011: 66-78.

[3] JIMENÉZ G A, BARAKOS G N. Accurate predictions of rotor hover performance at low and high disc loadings[J]. Journal of Aircraft, 2018, 55(3): 89-110.

[4] MCCUTCHEN C W. A theorem on swirl loss in propeller wakes[J]. Journal of Aircraft, 1985, 22(6): 344-346.

[5] FRANCOIS B, LABAN M, COSTES M D G. In-plane forces prediction and analysis in high-speed conditions on a contra-rotating open rotor[J]. Journal of Turbomachinery, 2014, 136(5): 1-16.

[6] JOHNSON W R. Helicopter theory[M]. New York: Dover Publications, 1994: 40-45.

[7] LUCAS F. Study of counter-rotating coaxial rotors in hover: a performance model based on blade element theory including swirl velocity[D]. Daytona Beach, US: Embry-Riddle Aeronautical University, 2007.

[8] STAHLHUT C, LEISHMAN J G. Aerodynamic design optimization of proprotors for convertible-rotor concepts [C]// 68th American Helicopter Society Annual Forum. Dallas, US: Vertical Flight Society, 2012: 593-616.

[9] MODARRES R, PETERS D A. Optimum actuator-disk performance in hover and axial flight by a compact momentum theory with swirl[J]. Journal of the American Helicopter Society, 2015, 60(4): 1-10.

[10] PETERS D A, HAQUANG N. Dynamic inflow for practical applications[J]. Journal of the American Helicopter Society, 1988, 33(4): 64-68.

[11] LEISHMAN J G. Principles of helicopter aerodynamics [M]. 3th ed. New York: Cambridge University Press, 2006: 62-64.

[12] HAN Dong, PASTRIKAKIS V, BARAKOS G N. Helicopter flight performance improvement by dynamic blade twist[J]. Aerospace Science and Technology, 2016, 58(2): 445-452.

[13] HAN Dong, DONG Chen, BARAKOS G N. Performance improvement of variable speed rotors by gurney flaps[J]. Aerospace Science and Technology, 2018, 81(5): 118-127.

[14] DONG Chen, HAN Dong, YU Lei. Performance analysis of variable speed tail rotors with gurney flaps[J]. Chinese Journal of Aeronautics, 2018, 31(7): 4-10.

[15] YEO H, BOUSMAN W G, JOHNSON W R. Performance

analysis of a utility helicopter with standard and advanced rotors[J]. Journal of the American Helicopter Society, 2004, 49(6): 250-270.

[16] SHINODA P M, YEO H, NORMAN T R. Rotor performance of a UH-60A rotor system in the NASA MES 80-by 120-foot wind tunnel[J]. Journal of the American Helicopter Society, 2004, 49(6): 401-413.

[17] HILBERT K B. A mathematical model of the UH-60 helicopter[R]. NASA-TM-85890, 1984.

[18] DAVIS S J. Pedesign study for a modern 4-bladed rotor for the RSRA[R]. NASA-CR-166155, 1981.

[19] JOHNSON W R. Rotorcraft aeromechanics [M]. New York: Cambridge University Press, 2013: 48-52.

[20] BUCKANIN R M, HERBST M K, LOCKWOOD R A, et al. Airworthiness and flight characteristics test of a sixth year production UH-60A[R]. Washington DC: USA AEFA Project No. 83-24, 1985.

[21] NAGATA J I, PIOTROWSKI J L, YOUNG C J, et al. Baseline performance verification of the 12th year production UH-60A black hawk helicopter[R]. Washington DC: USA AEFA Project No. 87-32, 1989.

[22] BOUSMAN W G. Power measurement errors on a utility aircraft[C]// Proceedings of 3rd American Helicopter Society Aerodynamics, Acoustics, and Test and Evaluation Technical Specialists Meeting. San Francisco, US: Vertical Flight Society, 2002: 35-48.

（编辑：陈　越）

JASP